Structural and magnetic properties of nanocomposites based on nanostructured polyaniline and titania nanotubes

M. Radoičić · G. Ćirić-Marjanović ·
Z. V. Šaponjić · M. Mitrić · Z. Konstantinović ·
M. Stoiljković · J. M. Nedeljković

Abstract Nanocomposites consisting of self-assembled polyaniline (PANI) nanostructures and titania nanotubes (TiO$_2$-NT) were synthesized by the oxidative polymerization of aniline with ammonium peroxydisulfate in an aqueous dispersion of TiO$_2$-NT (outer diameter $\sim$10 nm), without added acid. The influence of initial mole ratio of aniline to TiO$_2$ (80, 20, and 5) on the morphology, electrical conductivity, molecular structure, crystallinity, and magnetic properties of synthesized PANI/TiO$_2$ nanocomposites was studied. Transmission electron microscopy, Raman spectroscopy, and X-ray powder diffraction proved that the shape and structure of TiO$_2$-NT in the final nanocomposites were preserved. The shape of PANI nanostructures formed in the nanocomposites was influenced by the initial aniline/TiO$_2$-NT mole ratio. Nanotubes and nanorods are predominant PANI nanostructures in the nanocomposite prepared with the highest aniline/TiO$_2$ mol ratio of 80. The decrease of aniline/TiO$_2$ molar ratio induced more pronounced formation of nanorod network. The electrical conductivity of PANI/TiO$_2$ nanocomposites was in the range $(1.3–2.4) \times 10^{-3}$ S cm^{-1}. The nanocomposites exhibit weak ferromagnetic behavior. Approximately order of magnitude lower values of coercive field and remanent magnetization were obtained for nanocomposite samples in comparison to pure PANI.

M. Radoičić · Z. V. Šaponjić (✉) · M. Mitrić ·
M. Stoiljković · J. M. Nedeljković
Vinča Institute of Nuclear Sciences, University of Belgrade,
P.O. Box 522, 11001 Belgrade, Serbia
e-mail: saponjic@vinca.rs

G. Ćirić-Marjanović
Faculty of Physical Chemistry, University of Belgrade,
Studentski Trg 12-16, 11158 Belgrade, Serbia

Z. Konstantinović
Institut de Ciéncia de Materials de Barcelona, CSIC, Bellaterra,
08193 Barcelona, Spain

Introduction

Among conducting polymers, PANI is one of the most extensively studied due to its high conductivity, good environmental stability, simple preparation, low cost, wide applicability in sensors, electronic components, electrochromic devices, electrochemical capacitors, antistatic coatings, etc. [1]. Its electromagnetic and optical properties depend mostly on its oxidation state and protonation degree. In addition, unlike other conducting polymers PANI exhibits simple and reversible acid/base (doping/dedoping) chemistry. This fact opens-up possibility for better control over electrical and optical properties [2].

The properties of nanocomposites based on PANI and various metal and metal oxides nanoparticles can be simply modified by adjusting their ratio. For example, by incorporation of small amount of TiO$_2$ nanoparticles in PANI, its electrical, optical, magnetic, and sensing properties can be tuned. On the other hand, if TiO$_2$ nanoparticles are coated with a small amount of PANI, enhanced photocatalytic activity of TiO$_2$ in visible region is observed due to sensitizing capability of PANI [3]. The improvement of processability and conductivity of PANI in the nanocomposites based on PANI and TiO$_2$ nanoparticles was observed [4]. Also, specific morphologies, such as microspheres [5], nanotubes, and nanoribbons [6] were reported for these materials. These novel PANI/TiO$_2$ materials with improved properties find applications in various electronic devices, sensors, photocatalysis, and corrosion resistant coatings [4, 7–15].

In order to synthesize PANI/TiO$_2$ nanocomposites several methods have been used [9, 11, 15–21]. The most frequently employed technique is chemical oxidative polymerization of aniline in the presence of titanium dioxide nanoparticles [4, 6].

Properties of PANI/TiO$_2$ nanocomposites can be strongly influenced also by adding different dopant acids, surfactants, or by charging surface of TiO$_2$ nanoparticles during the polymerization process [19, 22–24].

Studying magnetic properties of PANI could provide significant information about charge-carrying species and unpaired spins in polymer chain. The method of polymer synthesis (e.g., doping level, dopant type) and measuring conditions (temperature, applied magnetic field) have a strong influence on magnetic susceptibility [25–27]. Although a numerous studies on magnetic properties of PANI are published just a few of them reported on ferromagnetic behavior. Ferromagnetism at room temperature for electrochemically synthesized PANI doped with large size functionalized dopant, 2,6-quinone disulfonic acid, was reported by Trivedi et al. [28]. Yoshizawa's group noticed ferromagnetic interaction between the spins at low temperature in PANI with meta coupled aniline units [29] and its *n*-dodecyl-substituted derivative [30]. Zaidi et al. [31] detected ferrimagnetic ordering at Curie temperature above 350 K in PANI–tetracyanoquinodimethane. Weak ferromagnetic response at temperatures below 50 K in nanocomposites based on PANI/para-toluene sulfonic acid (20 wt% TiO$_2$) was observed by Nagaraja et al. [32]. The meta/para coupling of repeated units in polymer can also yield to ferromagnetic spin alignment upon doping [33]. We have shown in our previous work that the room temperature ferromagnetic response with coercive field of $H_c \sim 300$ Oe and remanent magnetization of $M_r \sim 4.35 \times 10^{-4}$ emu g^{-1} was detected in all investigated PANI/TiO$_2$ nanocomposites synthesized by the oxidative polymerization of aniline in water, without added acid, in the presence of colloidal TiO$_2$ nanoparticles (content of TiO$_2$ nanoparticles was in the range 0.6–6.1 wt%) [34].

Besides the studying influence of TiO$_2$ crystal form on properties of PANI matrix within nanocomposite, the influence of shape of TiO$_2$ nanoparticles was also studied [35–38]. Cheng et al. showed that suspension of PANI/TiO$_2$ nanotubes composite possess a higher electrorheological activity than the suspension of PANI/TiO$_2$ composite prepared using sphere-like TiO$_2$ nanoparticles. Recently, Su et al. [36] showed that the addition of PANI layer on the top of electrochemically synthesized TiO$_2$-NT enhances the thermoelectric power and photosensitive properties. Electrochemically prepared PANI/TiO$_2$-NT nanocomposites also showed significant improvement in photoelectrocatalytic degradation of Rhodamine B in comparison with pure TiO$_2$-NTs [37].

In this work, conducting nanocomposites constituted of self-assembled PANI nanostructures and TiO$_2$-NTs have been prepared for the first time by the chemical oxidative polymerization of aniline in an aqueous dispersion of TiO$_2$-NTs, without added acid. The influence of TiO$_2$-NT content on the electrical, structural, morphological, and magnetic properties of PANI/TiO$_2$-NT nanocomposites was studied. Synthesized PANI/TiO$_2$-NT nanocomposites were studied by scanning electron microscopy (SEM), transmission electron microscopy (TEM), FTIR, and Raman spectroscopies, inductively coupled plasma optical emission spectroscopy (ICP-OES), XRD, and electrical conductivity measurements. In order to investigate the influence of TiO$_2$-NT on magnetic properties of PANI, magnetic susceptibility measurements were performed as a function of both, temperature (from room temperature down to 5 K) and magnetic field (-60 to 60 kOe).

Experimental

Materials

Aniline (p.a., >99.5 %, Centrohem, Serbia), was distilled under reduced pressure and stored at room temperature, under argon, prior to use. Ammonium peroxydisulfate (analytical grade, Centrohem, Serbia, APS) and TiO$_2$ (analytical grade, Fluka) were used as received.

Synthesis of TiO$_2$-NTs

Scrolled TiO$_2$-NTs were synthesized by a hydrothermal process (150 °C, 20 h) using as a precursor TiO$_2$ powder (Fluka) in alkaline (10 M NaOH) aqueous solution (250 mg/10 ml) [39]. After the synthesis TiO$_2$-NTs were washed until the pH of the suspension has reached seven and dried at 70 °C for 6 h.

Synthesis of PANI/TiO$_2$-NT nanocomposite

The aqueous solution of APS (0.4 M, 25 ml) was poured into the aqueous solution of aniline (0.32 M, 25 ml). Thereupon dispersions (50 ml) of various concentrations of TiO$_2$-NT in water were added into the aniline/APS solutions. In order to get stable dispersion of TiO$_2$-NT, ultrasonic bath (40 kHz) was used for 30 min. The mole ratios of aniline to TiO$_2$-NT were 80, 20, and 5, and these nanocomposites are designated as PT-NT-80, PT-NT-20, and PT-NT-5, respectively. The reaction mixture was stirred for 3 h at room temperature. The precipitated PANI/TiO$_2$-NT nanocomposite was collected on a filter, rinsed with ethanol acidified with sulfuric acid (5×10^{-3} M), and dried in vacuum at 60 °C for 3 h. As a reference sample,

pure PANI was prepared using the same procedure without TiO₂ (50 ml of distilled water was added into aniline/APS solution instead of the TiO₂-NT dispersion). The pH values of the starting reacting mixtures were in the range 6.0–6.5, while the final pH value was 1.3–1.5.

Characterization

A SEM JEOL JSM 6460 LV and a TEM Tecnai G2 Spirit (FEI, Brno, Czech Republic) were used to characterize the morphology of the PANI and PANI/TiO₂-NT samples. Powdered materials were deposited on adhesive tape fixed to specimen tabs and then ion sputter coated with gold using a BAL-TEC SCD 005 Sputter Coater prior to SEM measurements.

A TEM Hitachi H-7000 FA TEM with a W filament at a high tension of up to 125 kV was used to determine the sizes of the used TiO₂-NTs. The sample was prepared by drop-wise placing volume of 6 µl of TiO₂-NT aqueous dispersion onto a holey carbon film supported on a copper grid after 30 min of ultrasound treatment. The specimen was air-dried overnight.

The content of titanium in the PANI/TiO₂ nanocomposite was determined by ICP Emission Spectrometer: ICAP 6000 series (Thermo Electron Corporation), using the emission line Ti II 336.121 nm. Prior to ICP measurements, the powdered samples of PANI/TiO₂-NT (5 mg) were dispersed in 10 ml of concentrated H_2SO_4 and hydrothermally treated for 90 min at 250 °C in a Teflon vessel (Acid digestion bomb-Model 4746-Parr instrument).

The conductivity of PANI/TiO₂-NT powders compressed between stainless steel pistons was measured at room temperature by means of an ac bridge (Wayne Kerr Universal Bridge B 224), at fixed frequency of 1.0 kHz. During the measurement, pressure was maintained at ∼80 MPa.

FTIR spectra of the synthesized samples were recorded using Nicolet 380 FTIR spectrophotometer (Thermo Electron Corporation) in attenuated total reflection (ATR) mode. For each spectrum, 64 scans were performed, with a resolution of 2 cm⁻¹, in the range of 400–4000 cm⁻¹.

Raman spectra excited with a HeNe 633 nm gas laser were collected on a Thermo Scientific DXR Raman microscope, equipped with a research optical microscope and a CCD detector. The laser beam was focused on the sample placed on an X–Y motorized sample stage using objective magnification 50×. The scattered light was analyzed by the spectrograph with a grating 1200 lines mm⁻¹. Laser power was kept at 0.5 or 5.0 mW on the PANI/TiO₂-NT samples and at 5.0 mW on the pure TiO₂-NT sample.

The XRD patterns were obtained using a Philips PW 1050 powder diffractometer with Ni filtered Cu Kα radiation ($\lambda = 1.5418$ Å). The diffraction intensity was measured by the scanning technique in the 2θ range from 10 to 70° by a step size of 0.05° and a counting time of 50 s per step.

The field and temperature-dependent magnetizations of the powdered samples were measured with a superconducting quantum interference device magnetometer (Quantum Design).

Results and discussion

Course of polymerization

By monitoring the change of reaction temperature within the time frame of 3 h, it was possible to follow the oxidative polymerization reaction of aniline in water with APS, in the presence of TiO₂-NT. During this reaction, two well-developed exothermic phases separated by athermal period can be noticed, common for polymerization in water without added acid [37, 38], Fig. 1a. As can be seen in Fig. 1a, the presence of TiO₂-NT did not disturb the polymerization route of aniline, in general. In the course of polymerization of aniline molecules, sulfuric acid is produced. Consequently, the pH of the reaction mixture decreases and was recorded to estimate the progress of reaction (Fig. 1b).

The first exothermic phase corresponds to rapid oxidative oligomerization, while the second exothermic phase corresponds to the formation of polymer [6, 38]. At the beginning of the oxidation process, nonprotonated aniline molecules are in significant excess in comparison to anilinium cations. During the first exothermic polymerization phase the oxidized nonprotonated, linear and branched oligoanilines are formed [39–42]. The presence of TiO₂-NT in the reaction system did not induce neither acceleration nor slowing down of the first polymerization phase (Fig. 1).

Because the anilinium cation is much weaker reductant than nonprotonated aniline molecule [39–41], and the nonprotonated pernigraniline-like oligoanilines are much weaker oxidants than peroxydisulfate, the oxidative polymerization of remaining aniline/anilinium cations shows considerable slowdown until it is almost stopped at pH around 3.5. At this point, low-reactive anilinium cations became significantly prevalent over reactive nonprotonated aniline molecules. The reaction mechanism during the athermal polymerization phase is based on the very slow redox processes that include oxidation of nonprotonated aniline and anilinium cations with remaining peroxydisulfate and precipitated nonprotonated pernigraniline-like oligoanilines leading to the growth of nonprotonated pernigraniline-like oligoanilines [43]. During this phase, a slow decrease of pH value was detected (Fig. 1b). The
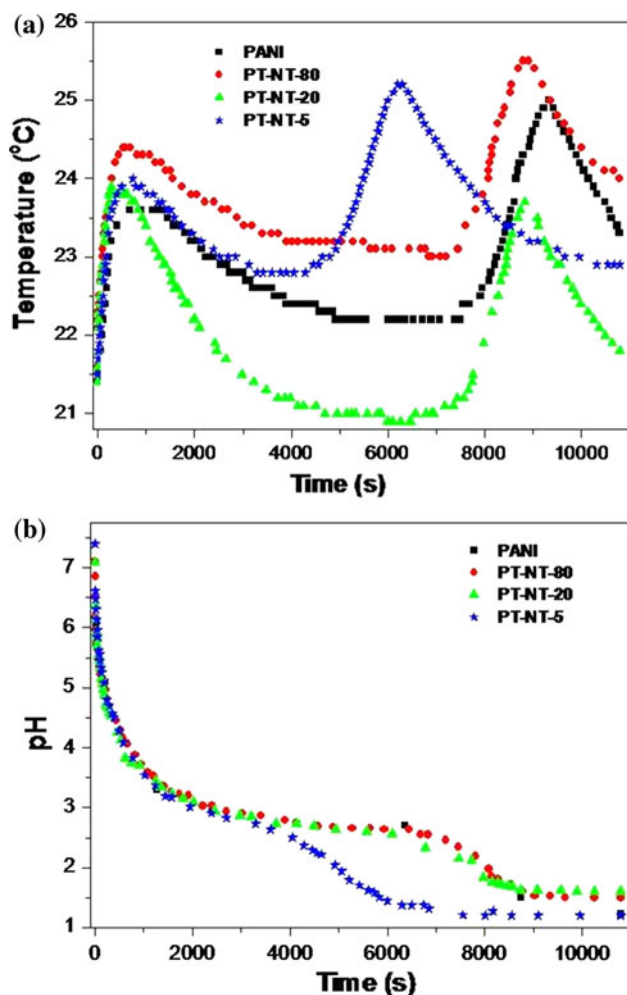
Fig. 1 a Temperature and **b** pH changes during the polymerization of aniline (0.08 M) with APS (0.1 M) in water: without added TiO$_2$-NT, and in the presence of different amounts of TiO$_2$-NT (synthesis of PT-NT-80, PT-NT-20, and PT-NT-5 nanocomposites)

presence of TiO$_2$-NT caused shortening of athermal phase (starting at pH < 3.5) compared to the corresponding phase in the synthesis of pure PANI (Fig. 1a), by accelerating mentioned redox reactions. Consequently, in the case of all nanocomposites, polymerization is completed faster than in the corresponding aniline oxidation without TiO$_2$-NTs. The shortest athermal period and the shortest overall reaction time was observed for the nanocomposite sample PT-NT-5 with the highest amount of TiO$_2$-NT. Similar results were obtained in our previous work on the nanocomposites consisted of PANI and colloidal TiO$_2$ nanoparticles [6]. The possible reason for such behavior could be a significant increase of the surface area of precipitated oligoanilines in the presence of nanotubular TiO$_2$. This is reflected in the increase of rate constants of reactions of dissolved and adsorbed aniline with pernigraniline-like oligoaniline. The specific surface area of precipitated oligoanilines contributes to the rate constants [44].

During the second exothermic phase of synthesis that begins after the athermal phase, at pH < 2.5, the protonation of completely oxidized pernigraniline-like oligomers takes place [6]. It causes the significant increase of their oxidant power and solubility [39, 40] leading to the autoacceleration of aniline polymerization. Beside the protonation by formed sulfuric acid, the protonation of completely oxidized pernigraniline-like oligomers by OH$_2^+$ groups present on the TiO$_2$-NTs surfaces in acidic conditions is also possible. Finally, the protonated, fully oxidized oligoanilines and residual peroxydisulfate will react with remaining nonprotonated aniline molecules, anilinium cations, and with reduced segments of partly oxidized oligoanilines also via the exothermic redox equilibrating process [6]. This reaction route leads toward the formation of PANI chains in the form of emeraldine salt (PANI sulfate/hydrogen sulfate).

Content of TiO$_2$-NT in PANI/TiO$_2$-NTs nanocomposites

The contents of titanium in the nanocomposites PT-NT-80, PT-NT-20, and PT-NT-5, determined by ICP-OES technique, were 0.6, 1.6, and 11.2 wt%, respectively. Based on these data, the contents of TiO$_2$ in the nanocomposites PT-NT-80, PT-NT-20, and PT-NT-5 were determined to be 1.0, 2.8, and 18.7 wt%, respectively. These results correspond reasonably well to the calculated content of TiO$_2$ in the nanocomposites from initial concentrations of components.

Morphology

TiO$_2$-NTs and PANI

Typical morphology of the TiO$_2$-NTs used for the synthesis of PANI/TiO$_2$-NT nanocomposites is shown in Fig. 2. An open-ended multiwall morphology of the scrolled
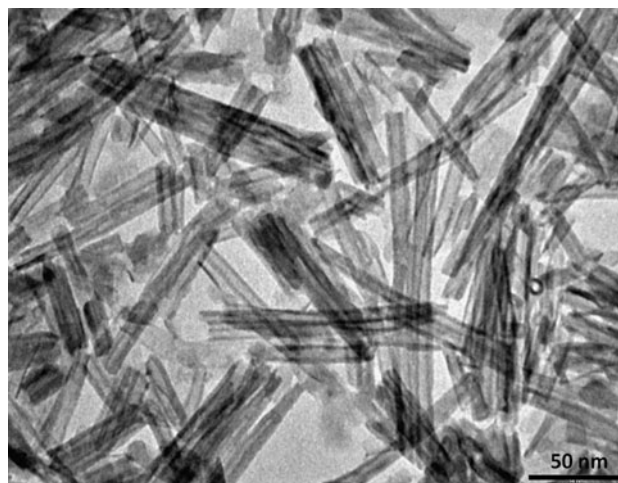

Fig. 2 TEM images of scrolled TiO$_2$-NTs

nanotubes was observed. The quite uniform size distribution of nanotube's outer and inner diameters (average size of about 10 and 7 nm, respectively) can be noticed, while length's distribution (up to few 100 nm) is much broader. The reference sample, pure PANI sulfate/hydrogensulfate, (prepared on the same manner, but without TiO$_2$-NTs) mainly consists of nanotubes (an average outer and inner diameter of 20–80 and 5–15 nm, respectively, and a length in the range from 0.3 to 3.0 μm)/nanorods, and nanoribbons (a thickness in the range of 50–140 nm), which are accompanied with the sheet-like objects with thickness of about 130–140 nm (Fig. 3a–c) [6].

PANI/TiO$_2$-NT nanocomposites

The changes in the morphology of the synthesized nanocomposites with the increase of the content of inorganic phase are studied by SEM and TEM (Figs. 3, 4). The morphology of the sample PT-NT-80, with the smallest content of TiO$_2$-NTs, is significantly different compared to the pure PANI sample. Nanotubes and nanorods of PANI are prevailing in the sample PT-NT-80, while nanoribbons are not observed (Fig. 3d–f). Nanotubes have an outer diameter of 60–150 nm, an inner diameter of 30–60 nm and a length up to few micrometers. An increase of the content of inorganic phase in the nanocomposites (samples PT-NT-20 and PT-NT-5) led to an enhanced connection of nanorods/nanotubes and formation of network (Figs. 3g–l, 4c, d). A detail with branching of PANI nanorods in PT-NT-5 nanocomposite is shown in Fig. 4d. The amount of PANI nanotubes, relative to PANI nanorods/nanofibers, is lowest in the sample with the highest content of inorganic phase (PT-NT-5). It means that the presence of TiO$_2$-NTs influenced the mechanism of aniline polymerization and consequently the probability of PANI nanotubes formation. It has been proposed that the formation of core (non-conducting oligoaniline)—shell (conducting PANI sulfate/hydrogen sulfate) structured nanorods is prerequisite step for PANI nanotubes formation [45]. The formation of PANI nanotubes is proposed to be a consequence of the dissolution of the cores of nanorods which is induced by the protonation of fully oxidized nonprotonated pernigraniline-like oligoanilines at pH < 2 [45]. The lowest content of PANI nanotubes can also be correlated with the shortest athermal period between two exothermic phases in T versus t curve for PT-NT-5 sample (Fig. 1a). The organization (self-assembling) of aniline oligomers, important for further formation of PANI nanostructures, is influenced by the presence of large amount of TiO$_2$-NTs, i.e., most probably by the interaction between aniline oligomers and TiO$_2$-NTs. The nanosheet/block-like objects were also observed in notable amount in the samples PT-NT-20 and PT-NT-5 (Figs. 3g, j, 4e).

It should be stressed that the original nanotubular morphology of TiO$_2$ is preserved upon the syntheses of nanocomposites, as shown in TEM images of PT-NT-20 (Figs. 3i, 4a, b) and PT-NT-5 (Fig. 4f) samples. The outer and inner diameters of TiO$_2$-NTs in the nanocomposites are close to those measured for pure starting TiO$_2$-NTs. The region with large amount of TiO$_2$-NTs in PT-NT-5 nanocomposite is shown in Fig. 4f.

Structural properties

FTIR spectroscopy

The presence of emeraldine salt form of PANI in all PANI/TiO$_2$-NT nanocomposite samples was proved by the FTIR spectroscopic analysis (Fig. 5). Bands that correspond to PANI emeraldine salt form were observed at 1569 cm^{-1} [quinonoid (Q) ring stretching vibration], 1497 cm^{-1} [benzene (B) ring stretching vibration], 1305 cm^{-1} (the C–N stretching vibration of secondary aromatic amine), 1246 cm^{-1} (the C–N$^{+\cdot}$ stretching vibration in polaron form of PANI emeraldine salt), 1146 cm^{-1} (the stretching vibration of –NH$^+$= in the B–NH$^+$=Q segment in bipolaron form of PANI emeraldine salt) and 826 cm^{-1} (the aromatic C–H out-of-plane deformation vibration of 1,4-disubstituted benzene ring, γ(C–H), in linear N–C4 coupled PANI chains) [38, 45–48]. The weak band at 880 cm^{-1} can be assigned to γ(C–H) vibration of 1,2,4-trisubstituted benzene ring, and indicates branching of PANI chains. The weak band at 1450 cm^{-1} can be assigned to the C=C stretching vibration of aromatic ring (most probably the monosubstituted and/or 1,2,4-trisubstituted rings) [48, 49].

Weak bands at 1635 and 1400 cm^{-1} which can be attributed to the substituted phenazine-like units were observed in the FTIR spectra of pure PANI and all nanocomposites [37, 46]. Although, in general, the bands in FTIR spectra of PANI/TiO$_2$-NT nanocomposites match the bands of pure PANI (Fig. 5), there is one exception. New band assigned to the phenazine-like segments appears at 1415 cm^{-1} in FTIR spectra of all nanocomposites. This feature is an indication that the presence of TiO$_2$-NTs during polymerization process affected intramolecular cyclization of branched nonprotonated oligoanilines which led to the formation of substituted phenazine-like units. The bands at 1042 and 590 cm^{-1} in the spectra of nanocomposites correspond to HSO$_4^-$ counter-ion, while the band at 618 cm^{-1} can be attributed to HSO$_4^-$ and/or SO$_4^{2-}$ counter-ions [48]. In the spectra of all investigated nanocomposites and pure PANI, two maxima within one broad band, at 1146 and 1120 cm^{-1} were observed. The maximum at 1120 cm^{-1} can be assigned to SO$_4^{2-}$ counter-ion vibration [48]. The asymmetric stretching vibration of SO$_3$ group in HSO$_4^-$ anions also contributes to the band at 1146 cm^{-1}.
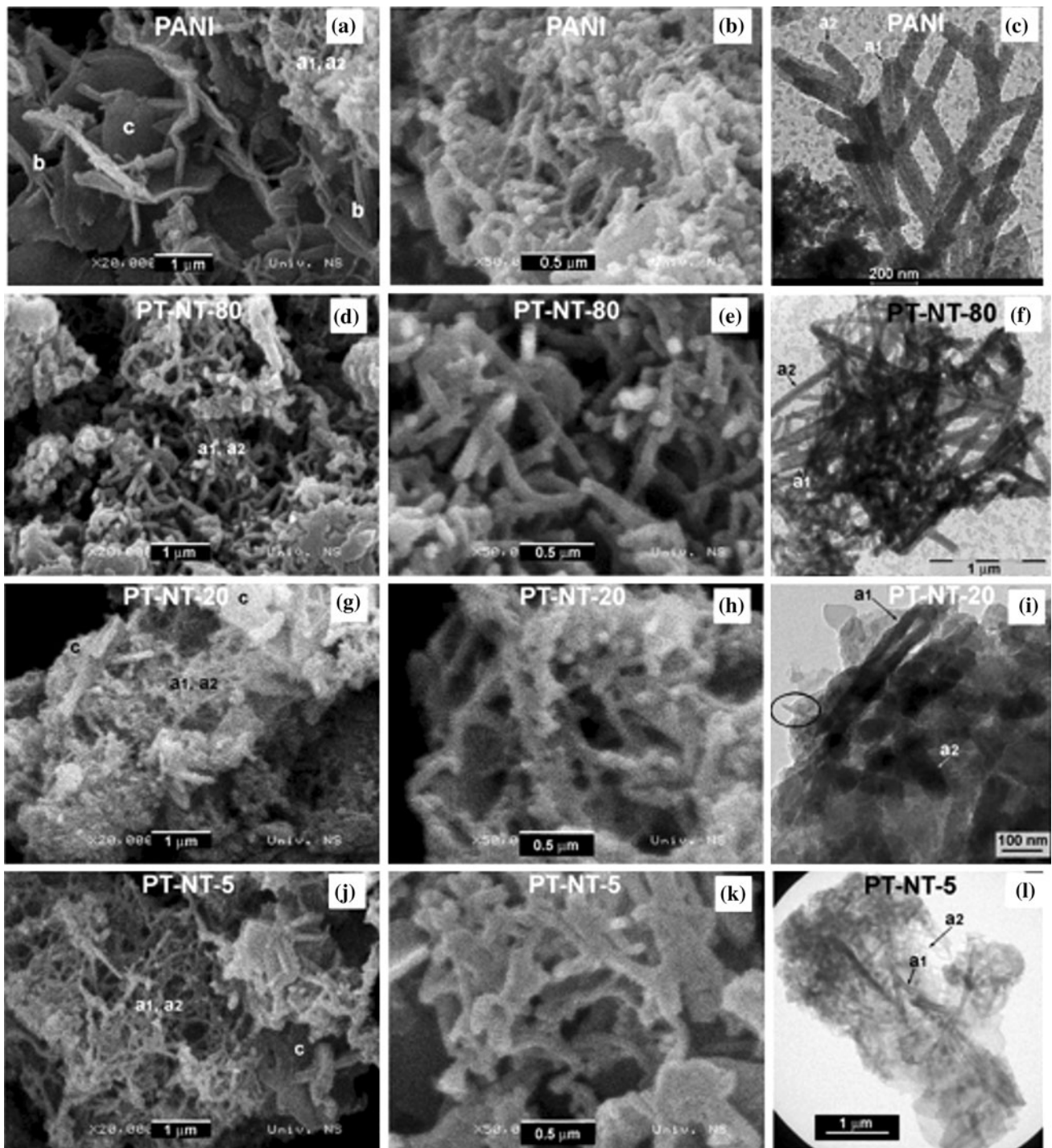
Fig. 3 SEM (**a**, **b**, **d**, **e**, **g**, **h**, **j**, **k**) and TEM (**c**, **f**, **i**, **l**) images of pure PANI (**a**, **b**, **c**), and PANI/TiO$_2$-NT nanocomposites PT-NT-80 (**d**, **e**, **f**), PT-NT-20 (**g**, **h**, **i**) and PT-NT-5 (**j**, **k**, **l**). PANI nanotubes and nanorods are designated with *a1* and *a2*, respectively (TEM images **c**, **f**, **i**, and **l**); nanoribbons in pure PANI are marked with *b* in image **a**; sheet-like structures are marked with *c* in images **a**, **g**, and **j**. A single TiO$_2$ nanotube is marked with an ellipse in image **i**

Raman spectroscopy

The Raman spectra of all nanocomposites, recorded with low laser power (0.5 mW) to avoid the degradation of PANI, are almost identical and exhibit only the characteristic bands of PANI (Fig. 6). The characteristic bands of TiO$_2$-NT were not observed due to low content of inorganic phase compared to PANI and probably due to insufficient laser power (Fig. 6). The bands that belong to PANI emeraldine salt structural units [42] are observed at
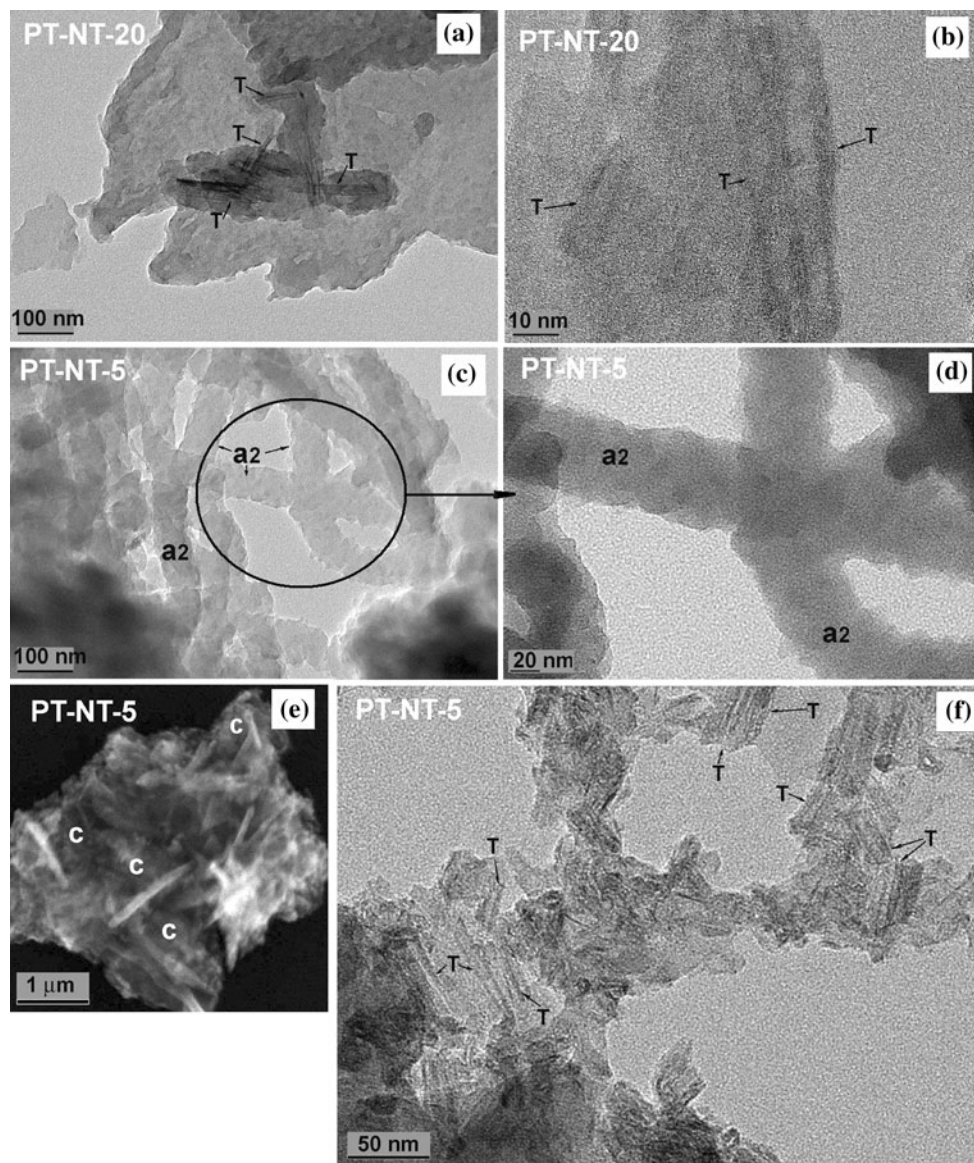
Fig. 4 TEM images with morphological details of PT-NT-20 (**a**, **b**) and PT-NT-5 (**c–f**) nanocomposites: TiO₂-NTs are marked with *T* in images **a**, **b** and **f**; PANI nanorods are marked with *a2* in images **c** and **d** (image **d** shows an enlarged part of image **c** with branching site in a nanorod network); PANI nanosheets are marked with *c* in image **e**

about 1596 cm^{-1} (the C=C and C$\sim$C stretching vibrations of the quinonoid and semi-quinonoid (SQ) rings, respectively, where '$\sim$' denotes the bond intermediate between the single and double bond), 1342 cm^{-1} (the C$\sim$N$^{+\cdot}$ stretching vibration of delocalized polaronic structure), 1260 cm^{-1} (the C–N stretching in benzene units) and 1170 cm^{-1} (the C–H bending in-plane vibration of SQ rings).

The bands observed at 1566, 1402, 1360, and 578 cm^{-1} are associated with the substituted phenazine structural units in PANI [42]. The phenazine-like units have been previously found to be important for the self-assembly of PANI nanotubes and nanorods [40–42, 45]. The peak

observed at 1640–1645 cm^{-1} corresponds to the C$\sim$C stretching vibrations of benzene units, with possible contribution of substituted phenazine units. When higher laser power (5.0 mW) was applied to the nanocomposite sample PT-NT-80, the part of spectrum that correspond to PANI has changed due to the partial degradation/crosslinking of PANI caused by laser irradiation, while, on the other side, several characteristic bands of TiO₂-NT become visible at 274, 435, 665 ,and 914 cm^{-1}. These bands are positioned close to wavenumbers that correspond to the Raman spectrum of pure TiO₂-NT (275, 445, 664, and 913 cm^{-1}), proving that the structure of TiO₂-NT was preserved upon aniline polymerization (Fig. 6). The Raman spectrum of
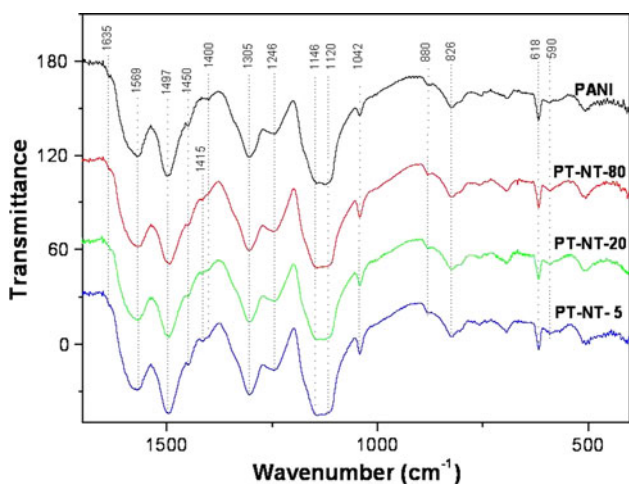
Fig. 5 FTIR spectra of pure PANI and PANI/TiO$_2$-NT nanocomposites PT-NT-80, PT-NT-20, and PT-NT-5
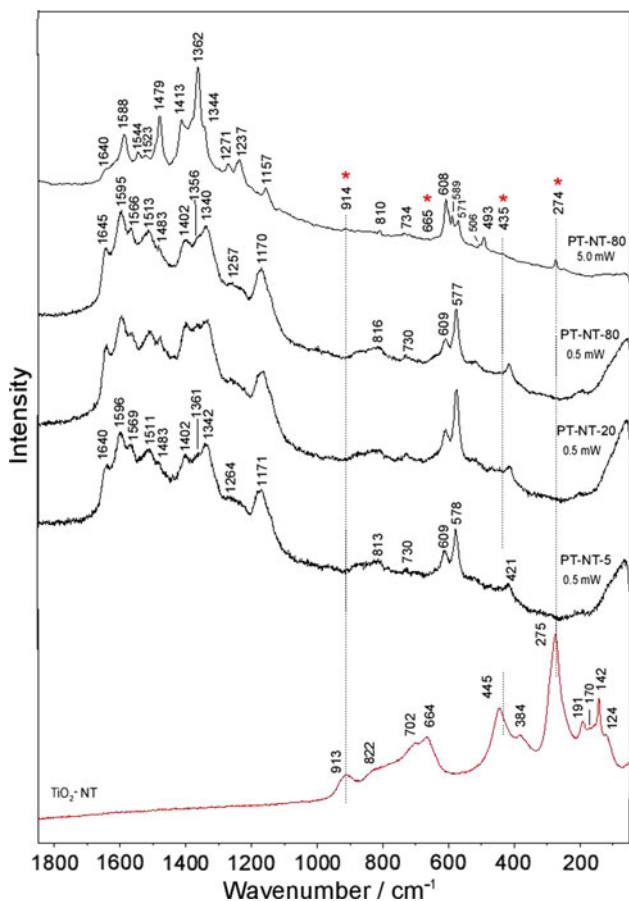

Fig. 6 Raman spectra of PANI/TiO$_2$-NT nanocomposites PT-NT-80, PT-NT-20 and PT-NT-5 recorded with excitation wavelength 633 nm and laser power of 0.5 or 5.0 mW. The spectrum of pure TiO$_2$-NT is also shown for comparison

synthesized TiO$_2$-NTs is in agreement with the published data concerning Raman spectra of TiO$_2$-NTs synthesized by the same or similar hydrothermal/soft chemical methods [50, 51].

XRD

Crystallinity of PANI depends on the conditions of preparation/processing and its protonation level [52, 53]. Doping of PANI by various acids causes the arrangement of polymer chains in highly ordered structures, due to the dopant-polymer interactions. Conducting PANI emeraldine salt form is semi-crystalline, containing crystalline and amorphous domains, while the PANI emeraldine base is predominantly amorphous [53]. Furthermore, incorporation of nanofillers into polymer matrix also has an influence on crystallinity of polymer chains.

The XRD patterns of pure PANI sulfate/hydrogen sulfate, TiO$_2$-NT and PANI/TiO$_2$-NT nanocomposite samples are shown in Fig. 7. The TiO$_2$-NTs are characterized by quasianatase, axially symmetric, and distorted octahedral coordination with a large fraction of five-coordinated sites on the surface [54]. In the XRD spectrum of the TiO$_2$-NTs, diffraction peaks characteristic for the anatase structure with modified cell parameters were observed at 9.5, 24.1, 28.3, and 48.2°. A common feature of the crystal forms of the anatase TiO$_2$ and titanate, which are usually assigned to the nanotubes, is that consist of the octahedra which shares four edges and zigzag chains joined together forming layers [55].

All the nanocomposite samples and pure PANI exhibit well-developed crystalline peaks superimposed on a broad scattering background that is characteristic of crystalline regions within an amorphous medium.

Diffraction patterns of nanocomposites contain the peaks at 9.5 and 48.2° characteristic for TiO$_2$-NT. Intensity of these peaks in nanocomposite samples, as expected, increases with the increase of TiO$_2$-NT content. The peak which appears at 24.1° in the XRD pattern of pure TiO$_2$-NT was detected only in the case of PT-NT-5 nanocomposite sample with the largest content of TiO$_2$-NT. In the case of nanocomposite with the smallest amount of TiO$_2$-NT (PT-NT-80) the peaks corresponding to nanoribbons and nanosheets of PANI are observed at 17.7, 19.0, and 25.9° along with the peaks at 23.0 and 28.0° assigned to the periodicity caused by π–π stacking of phenazine-like structures [34, 56, 57]. Relative intensity of the peak at ~17.7° is lower in the diffractograms of all nanocomposites compared to that in the diffractogram of pure PANI sample. The increase of the content of inorganic phase in the nanocomposite did not cause substantial changes in the diffractogram of PT-NT-20. However, the XRD pattern of the nanocomposite sample with the highest amount of TiO$_2$-NT (PT-NT-5) differs from the patterns of other samples. First, it shows the lowest intensity of the peaks at 23.0 and 28.0°. This feature indicates smaller contribution of phenazine-type structures and it can be correlated with the low content of tubular PANI forms, which is in
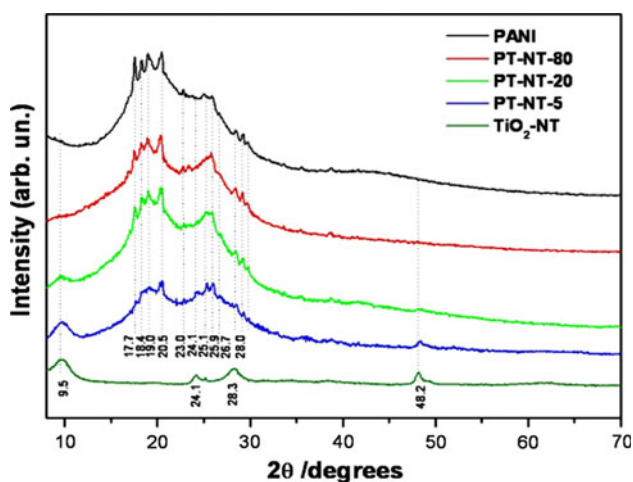
Fig. 7 XRD patterns of powdered samples of pure PANI, TiO$_2$-NTs, PT-NT-80, PT-NT-20, and PT-NT-5 nanocomposites

agreement with TEM data. Further, the intensities of the peaks at 17.7 and 19°, related to the nanoribbons, nanosheets and the layered oligomeric tetramers [56], are significantly decreased in XRD pattern of PT-NT-5. On the other hand, the broad peaks at 20.0 and 25.0°, characteristic of ordinary PANI and attributed to the periodicity parallel and perpendicular to the polymer chain of PANI, respectively, preserved their intensity in all samples [34, 58]. However, while the peak at 20.0° is more intensive then the peak at 25.0° in the case of nanocomposites with smaller content of inorganic phase (PT-NT-80 and PT-NT-20), these two peaks have almost the same intensities in the PT-NT-5 sample. The decrease of intensity of the peak at 20.0° relative to the peak at ∼25° in the XRD pattern of the sample PT-NT-5 implies that TiO$_2$-NTs, present in the highest amount, induced much less pronounced periodicity in direction parallel to the polymer chain. On the other hand, these results suggest that the extent of ordering perpendicular to the polymer chain does not depend significantly on the amount of TiO$_2$-NTs in the nanocomposites.

According to Bhadra et al., the PANI peaks at 18.4, 19.0, 20.5, 25.1, and 25.9° observed in XRD spectra of nanocomposites in Fig. 7 can be attributed to d$_{-111}$, d$_{200}$, d$_{0-41}$/d$_{011}$, d$_{040}$, and d$_{3-40}$ planes in triclinic crystal structure with P1 space group symmetry [59].

Conductivity

Polyaniline/TiO$_2$-NT nanocomposite samples show electrical conductivity on a semiconducting level, which is slightly dependent on the content on inorganic phase. The conductivity ($\sigma = 1.3 \times 10^{-3}$ S cm^{-1}) of the sample with the largest amount of TiO$_2$-NT (PT-NT-5) was slightly higher than the conductivity of pure PANI sample

($\sigma = 9.0 \times 10^{-4}$ S cm^{-1}). The decrease of the content of inorganic phase in nanocomposites induced increase of conductivity (2.4×10^{-3} and 1.9×10^{-3} S cm^{-1} for PT-NT-20 and PT-NT-80, respectively).

Magnetic properties

The diamagnetic contribution to the total magnetization determined from the field dependence of magnetization at room temperature is observed in all samples (not shown). The same order of magnitude was obtained for the net mass magnetization of pure PANI and PANI/TiO$_2$-NT nanocomposites.

The temperature-dependent magnetic susceptibility, after diamagnetic correction, at magnetic field of 10 kOe is shown in Fig. 8. The nearly temperature-independent Pauli susceptibility from room temperature down to 100 K and Curie-like susceptibility at low temperature (below 50 K) were observed. The total magnetic susceptibility, χ_{para}, can be described by:

$$\chi_{para} = \chi_{Pauli} + C/T$$

where C is the Curie constant [25].

The dependence of Pauli-like susceptibility and Curie constant on the amount of TiO$_2$-NT in PT-NT nanocomposites is shown in Fig. 9. The Pauli-like susceptibility is usually attributed to the delocalized spins in metallic crystalline region of polymer, while the Curie-like contribution is associated with trapped spins strongly localized to single polymer chain or defects in amorphous regions [25, 59]. The Curie constant and the Pauli-like susceptibility
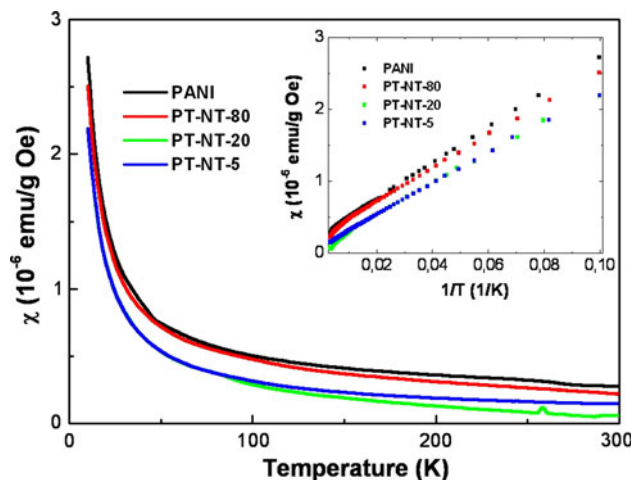

Fig. 8 Temperature dependence of paramagnetic susceptibility for pure PANI and PANI/TiO$_2$ nanocomposites (PT-NT-80, PT-NT-20, PT-NT-5); Inset: χ versus 1/T. "Copyright 2012 Wiley; the data for pure PANI adapted with permission from Ref. [34], Radoičić et al., Ferromagnetic PANI/TiO$_2$ nanocomposites, Polymer Composites, John Wiley and Sons"
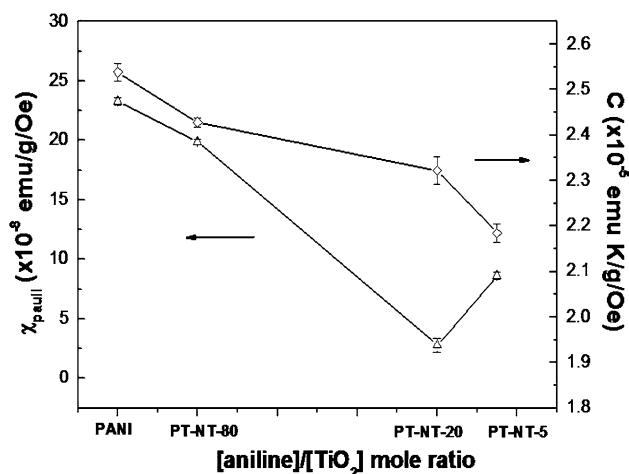
Fig. 9 The dependence of Currie constant and the Pauli-like susceptibility on the amount of TiO$_2$-NT for different PANI/TiO$_2$ nanocomposites and pure PANI

decreases with increasing the amount of TiO$_2$-NTs in nanocomposites compared to the pure PANI.

The observed decrease of the Pauli-like susceptibility is the consequence of decreased spin delocalization induced by reduced average chain conjugation length and higher torsion angles in structural features such as 1,2,4-trisubstituted and 1,2,4,5-tetrasubstituted rings, branched polymer chains and phenazine-like segments which are non-typical for standard PANI. Their presence in PANI/TiO$_2$-NT nanocomposites was confirmed by FTIR, Raman, and XRD measurements.

The field dependence magnetization after diamagnetic correction is shown in Fig. 10. At low temperature, the Curie susceptibility is dominant (Fig. 10a). However, the weak ferromagnetic behavior can be observed in all samples (Fig. 10b).

Pure PANI sample showed hysteresis loop with the coercive field of $H_c \sim 300$ Oe and remanent magnetization of $M_r \sim 4.35 \times 10^{-4}$ emu g^{-1} (see inset to Fig. 10a). The observed weak ferromagnetic behavior persist up to room temperature with the saturation magnetization about $M_s \sim 2 \times 10^{-3}$ emu g^{-1} (see Fig. 10b). The presence of single-charged polarons with spin ($S = 1/2$) located at the nitrogen [29] within PANI structures could explain the observed ferromagnetic ordering, through the π conjugation over the phenyl rings.

In comparison to pure PANI sample, PANI/TiO$_2$-NT nanocomposite samples exhibit much weaker ferromagnetic ordering. Saturation magnetization was approximately $M_s \sim 2.5 \times 10^{-4}$ emu g^{-1} with almost closed hysteresis loop (see Fig. 10b). The presence of TiO$_2$-NTs in investigated concentration range in PANI-based nanocomposites reduced several times the saturation magnetization value. In general, the decrease of the saturation magnetization value could be the consequence of the
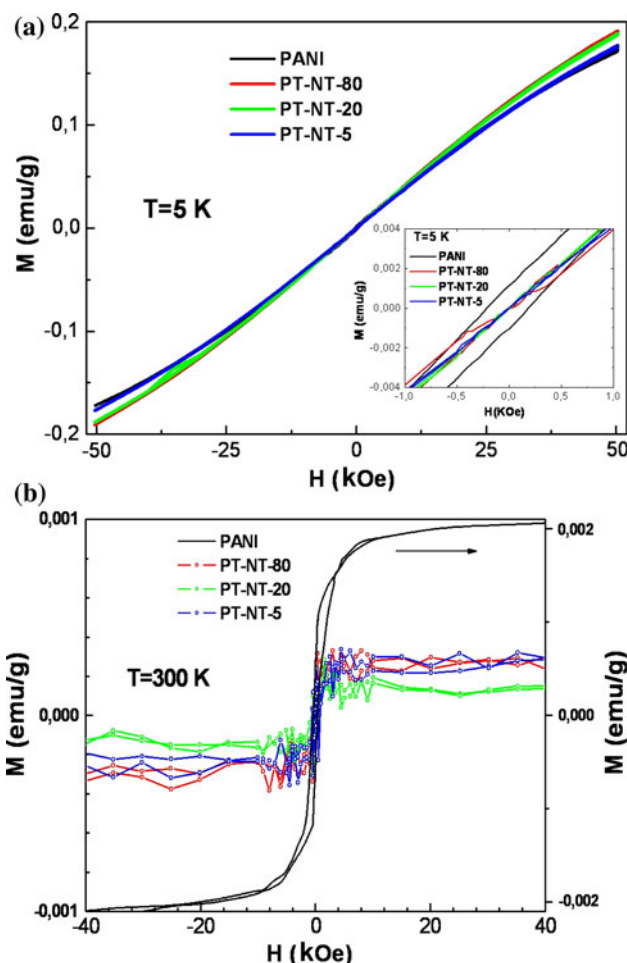

Fig. 10 The magnetic field dependence of magnetization after diamagnetic correction at **a** 5 K and **b** 300 K for the pure PANI and PANI/TiO$_2$ nanocomposite samples (PT-NT-80, PT-NT-20, PT-NT-5). "Copyright 2012 Wiley; the data for pure PANI adapted with permission from Ref. [34], Radoičić et al., Ferromagnetic PANI/TiO$_2$ nanocomposites, Polymer Composites, John Wiley and Sons"

increased spin disordering as well as the reduction of the total number of magnetic moments. The reason for decrease of ferromagnetism in nanocomposite samples is conversion of single-charged polarons into double-charged bipolarons ($S = 0$) induced by the presence of TiO$_2$-NTs. Taking into account an earlier investigation on conjugated systems which supposed that extensive spin stabilization can be achieved using branched oligomers to yield a two-dimensional network with meta/para coupling [33], observed branching and the presence of phenazine-like units in PANI chains seems to be of crucial importance for observed ferromagnetism in pure PANI samples [33, 34]. Even the smallest amount of titania nanotubes (PT-NT-80) caused disordering and delocalization of single-charged polarons. In light of the foregoing, the decreased ferromagnetism in the PANI/TiO$_2$-NT nanocomposites at room temperature is most likely induced by decreased extent of branching in oligoanilines and decreased the content/

absence of 2-D nanostructures (nanosheets/nanoribbons), taking into account the results of XRD and SEM/TEM measurements. TiO$_2$-NTs may also affect the interchain interactions and change the structural ordering of PANI part in the composites, leading thus to the observed weaker ferromagnetic behavior of PANI/TiO$_2$-NT composites.

It should be pointed out that significant decrease of the room temperature ferromagnetic ordering in PANI/TiO$_2$-NT nanocomposites compared to that of pure PANI was not observed when the composites were prepared with the colloidal TiO$_2$ nanoparticles [34]. The PT-NT-80 nanocomposite, containing 1.0 wt% of TiO$_2$ nanotubes, exhibited much weaker ferromagnetism then the pure PANI, while the PANI/TiO$_2$ nanocomposites which were prepared by analogous procedure but in the presence of the similar or higher content (0.6–6.1 wt%) of colloidal TiO$_2$ nanoparticles exhibited ferromagnetism comparable to that of pure PANI ($M_r \sim 4.35 \times 10^{-4}$ emu g^{-1} and coercive field of $H_c \sim 300$ Oe) [34]. In the light of the foregoing, it is clear that the ferromagnetic ordering in PANI/TiO$_2$ nanocomposites, prepared by the same procedure greatly depends on the shape of TiO$_2$ nanoparticles.

Conclusions

In this work, novel nanocomposites consisting of PANI nanostructures and TiO$_2$-NTs were synthesized by the oxidative polymerization of aniline with APS in aqueous medium in the presence of TiO$_2$-NTs, without added acid. The nanocomposites synthesized at aniline/TiO$_2$ mol ratios of 80, 20, and 5 contain 1.0, 2.8, and 18.7 wt% of TiO$_2$-NTs, respectively. The significant acceleration of the overall polymerization of aniline was observed in the presence of the highest concentration of TiO$_2$-NTs. TEM, Raman, and XRD techniques confirmed that the original shape and structure of TiO$_2$ nanotubes are preserved in the nanocomposites. PANI nanotubes and nanorods prevail in the sample with the lowest content of TiO$_2$-NTs (1.0 wt%). Branching of nanorods is pronounced when the amount of TiO$_2$-NTs increases, leading to the formation of nano-network. The relative amount of PANI nanotubes is lowest in the sample with the highest content of TiO$_2$-NTs (18.7 wt%). FTIR and Raman spectroscopies of the nanocomposites revealed the presence of emeraldine salt form, as well as phenazine-like segments in PANI chains. Besides the peaks of ordinary (granular) PANI, XRD patterns of nanocomposites exhibit additional peaks that can be attributed to different PANI nanostructures and unordinary segments (e.g., phenazine-type). The decrease of the content of inorganic phase in the nanocomposites induced increase of the electrical conductivity from 1.3×10^{-3} S cm^{-1} for the sample with 18.7 wt% of TiO$_2$-NTs to slightly more than 2×10^{-3} S cm^{-1} for the samples

with 2.8 and 1.0 wt% of TiO$_2$-NTs. Significantly weaker room temperature ferromagnetic ordering in PANI/TiO$_2$-NT nanocomposite samples compared to pure PANI sulfate/hydrogensulfate was observed. The almost closed hysteresis loops and $M_s \sim 2.5 \times 10^{-4}$ emu g^{-1} are observed in all nanocomposite samples. The synthesized PANI/TiO$_2$-NT composites constitute novel materials which may be considered in relation to potential applications, such as photocatalysts, electronic components, sensors, or corrosion resistant coatings.

References

1. Wallace GG, Spinks GM, Kane-Maguire LAP, Teasdale PR (2003) Conductive electroactive polymers: intelligent materials systems. CRC Press, Boca Raton
2. Lee K, Cho S, Park SH, Heeger AJ, Lee CW, Lee SH (2006) Nature 44:65
3. Li X, Wang D, Cheng G, Luo Q, An J, Wang Y (2008) App Catal B: Environ 81:267
4. Su SJ, Kuramoto N (2000) Synth Met 114:147
5. Zhang L, Wan M, Wei Y (2005) Synth Met 151:1
6. Radoičić M, Šaponjić Z, Nedeljković J, Ćirić-Marjanović G, Stejskal J (2010) Synth Met 160:1325
7. Somani PR, Marimuthu R, Mulik UP, Sainkar SR, Amalnerkar DP (1999) Synth Met 106:45
8. Ma L, Li Y, Yu X, Zhu N, Yang Q, Noh CH (2008) J Solid State Chem 12:1503
9. Xia H, Wang Q (2002) Chem Mater 14:2158
10. Ameen S, Akhtar MS, Kim GS, Kim YS, Yang OB, Shin HS (2009) J Alloy Compd 487:382
11. Zhang H, Zong R, Zhao J, Zhu Y (2008) Environ Sci Technol 42:3803
12. Roy AS (2011) J Appl Polym Sci 121:675
13. Gong J, Li YH, Hu ZS, Zhou ZZ, Deng YL (2010) J Phys Chem C 114:9970
14. Sathiyanarayanan S, Syed Azim S, Venkatachari G (2007) Synth Met 157:205
15. Radhakrishnan S, Siju CR, Mahanta D, Patil S, Madras G (2009) Electrochim Acta 54:1249
16. Karim MR, Lee HW, Cheong IW, Park SN, Oh W, Yeum JH (2010) Polym Comp 31:83
17. Xiong SX, Wang Q, Xia HS (2004) Synth Met 146:37
18. Sui XM, Chu Y, Xing SX (2004) Mater Lett 58:1255
19. Yavuz AG, Gok A (2007) Synth Met 157:235
20. Karim MR, Yeum JH, Lee MS, Lim KT (2008) React Funct Polym 68:1371
21. Schnitzler DC, Zarbin AJG (2004) J Braz Chem Soc 15:378
22. Zhang L, Wan M (2003) J Phys Chem B 107:6748
23. Kim BS, Lee KT, Huh PH, Lee DH, Jo NJ, Lee JO (2009) Synth Met 159:1369
24. Xiong S, Phua SL, Dunn BS, Ma J, Lu X (2010) Chem Mater 22:255

25. Long Y, Chen Z, Shen J, Zhang Z, Zhang L, Xiao H, Wan M, Duvail JL (2006) J Phys Chem B 110:23228
26. Raghunathan A, Natarajan TS, Rangarajan G, Dhawan SK, Trivedi DC (1993) Phys Rev B 47:13189
27. Ginder JM, Richter AF, Mac Diarmid AG, Epstein AJ (1987) Solid State Commun 63:97
28. Trivedi DC (2001) Synth Met 121:1780
29. Yoshizawa K, Tanaka K, Yamabe T, Yamauchi J (1992) J Chem Phys 96:5516
30. Ito A, Ota K, Tanaka K, Yamabe T, Yoshizawa K (1995) Macromolecules 28:5618
31. Zaidi NA, Giblin SR, Terry I, Monkman AP (2004) Polymer 45:5683
32. Nagaraja M, Pattar J, Shashank N, Manjanna J, Kamada Y, Rajanna K, Mahesh HM (2009) Synth Met 159:718
33. Bushby RJ, McGill DR, Ng KM, Taylor N (1997) J Mater Chem 7:2343
34. Radoičić M, Šaponjić Z, Ćirić-Marjanović G, Konstantinović Z, Mitrić M, Nedeljković J (2012) Polym Compos 33:1482
35. Cheng Q, Pavlinek V, He Y, Li C, Saha P (2009) Colloid Polym Sci 287:435
36. Su L, Gan YX (2012) Compos B 43:170
37. Gospodinova N, Mokreva P, Terlemezyan L (1993) Polymer 34:2438
38. Trchová M, Konyushenko EN, Stejskal J, Sedenková I, Holler P, Ćirić-Marjanović G (2006) J Phys Chem B 110:9461
39. Ćirić-Marjanović G, Trchová M, Stejskal J (2006) Collect Czech Chem Commun 71:1407
40. Ćirić-Marjanović G, Trchová M, Stejskal J (2008) Int J Quantum Chem 108:318
41. Ćirić-Marjanović G, Konyushenko EN, Trchová M, Stejskal J (2008) Synth Met 158:200
42. Ćirić-Marjanović G, Trchová M, Stejskal J (2008) J Raman Spectrosc 39:1375
43. Ćirić-Marjanović G, Dragičević Lj, Milojević M, Mojović M, Mentus S, Dojčinović B, Marjanović B, Stejskal J (2009) J Phys Chem B 113:7116
44. Gill MT, Chapman SE, DeArmitt CL, Baines FL, Dadswell CM, Stamper JG, Lawless GA, Billingham NC, Armes SP (1998) Synth Met 93:227
45. Janošević A, Ćirić-Marjanović G, Marjanović B, Holler P, Trchová M, Stejskal J (2008) Nanotechnology 19:135606
46. Stejskal J, Sapurina I, Trchová M, Konyushenko EN, Holler P (2006) Polymer 47:8253
47. Kang ET, Neoh KG, Tan KL (1998) Prog Polym Sci 23:277
48. Socrates G (2001) Infrared and Raman characteristic group frequencies: tables and charts. Wiley, New York
49. Vien DL, Colthup NB, Fateley WG, Grasselli JG (1991) The handbook of infrared and Raman characteristic frequencies of organic molecules. Academic, San Diego
50. Yao BD, Chan YF, Zhang XY, Zhang WF, Yang ZY, Wang N (2003) Appl Phys Lett 82:281
51. Qian L, Du ZL, Yang SY, Jin ZS (2005) J Mol Struct 749:103
52. Djurado D, Nicolau YF, Rannou P, Luzny W, Samuelsen EJ, Terech P, Bée M, Sauvajol JL (1999) Synth Met 101:764
53. Pouget JP, Józefowicz ME, Epstein AJ, Tang X, MacDiarmid AG (1991) Macromolecules 24:779
54. Šaponjić ZV, Dimitrijević NM, Tiede DM, Goshe AJ, Zuo X, Chen LX, Barnard AS, Zapol P, Curtiss L, Rajh T (2005) Adv Mater 17:965
55. Zhu HY, Lan Y, Gao XP, Gao SP, Ringer SP, Zheng ZF, Song DY, Zhao JC (2005) J Am Chem Soc 127:6730
56. Laslau C, Ingham B, Zujovic ZD, Capkova P, Stejskal J, Trchová M, Travas-Sejdic J (2012) Synth Met 161:2739
57. Zujovic ZD, Laslau C, Bowmaker GA, Kilmartin PA, Webber AL, Brown SP, Travas-Sejdic J (2010) Macromolecules 43:662
58. Zhang L, Wan M (2003) Adv Funct Mater 13:815
59. Bhadra S, Singha NK, Khastgir D (2007) J Appl Polym Sci 104:1900